PAPER • **OPEN ACCESS**

Characterization of monolayer WSe_2 sandwiched in a hetero-plasmonic dimer

To cite this article: Priyanka Suri *et al* 2022 *Nano Ex.* **3** 045001

IOP Publishing Nano Express 3 (2022) 045001 https://doi.org/10.1088/2632-959X/ac9c78

NANO EXPRESS

PAPER

Characterization of monolayer WSe_2 sandwiched in a hetero-plasmonic dimer

Priyanka Suri[1,*], **Preeti Deshpande**[1] and **Ambarish Ghosh**[1,2]

[1] Centre for Nano Science and Engineering, Indian Institute of Science, Bengaluru, Karnataka, India
[2] Department of Physics, Indian Institute of Science, Bengaluru, Karnataka, India
[*] Author to whom any correspondence should be addressed.

E-mail: priyankasuri@iisc.ac.in **and** ambarish@iisc.ac.in

Keywords: plasmonics, 2D materials, Raman/PL, spectroscopy, strain and doping, single photon emission

Supplementary material for this article is available online

OPEN ACCESS

RECEIVED
26 July 2022

REVISED
26 August 2022

ACCEPTED FOR PUBLICATION
20 October 2022

PUBLISHED
7 November 2022

Abstract

Recent interests in layered transition-metal dichalcogenides (TMDCs), such as WSe_2, MoS_2, etc, arise due to their attractive electrical, optical, and mechanical properties with potential applications in energy storage, generation, and many more. Embedding these 2D materials in plasmonic cavities can further enhance light–matter interactions and alter their properties, resulting in diverse and efficient optoelectronic applications. The strain due to the geometry and charge transfer due to the plasmonic materials can further modify the TMDCs' optical response for sensing applications and as single photon emitters in on-chip optoelectronic applications. This work discusses one such 2D-plasmonic hybrid configuration of a silver sphere on a gold disc with WSe_2 sandwiched in between. We perform non-invasive Raman and PL studies of this system to estimate the field enhancement and discuss strain and doping induced in the TMDC.

Introduction

Metal nanoparticles of different shapes, sizes, and materials like gold (Au), Silver (Ag), or Copper (Cu) show strong interaction with incident light through the excitation of collective and coherent electron oscillations known as localized surface plasmons. Applications include surface-enhanced Raman spectroscopy (SERS), photovoltaics, photocatalysis, and many more, making noble metal nanoparticles attractive for fundament studies as well as technologically important [1–7]. The strength of these electromagnetic couplings depends on the number of such nanoparticles and their separation distance. Of all plasmonic systems, the most common is a two-nanoparticle system with nm and smaller spacings in between, also known as dimers, which has great scope in biological imaging, photodetection, and optical sensing, along with those mentioned above. The easiest way of maintaining such a sub-nm gap is by placing a material of equal thickness between the plasmonic particles. In this respect, two-dimensional materials like graphene and transition metal dichalcogenides (TMDCs) with atomic thickness have found much attention [8–14]. Previously we have shown how sandwiching a single layer of graphene between two silver nanoparticles resulted in unprecedented photoresponsivity in graphene that allowed the realization of a new class of large-area color-selective plasmonic photodetector at room temperature [15]. The local electromagnetic field at the junction of the sub-nm spaced dimers increased dramatically, thereby resulting in the most sensitive graphene–plasmonic hybrid photodetector reported to date. Such an architecture signifies the tremendous promise of integrating plasmonics with atomically thin materials, especially TMDCs, in nanoelectronics and nanophotonic applications [15–19, 44], arising due to the direct bandgap of TMDC monolayers in the visible region.

It is necessary to recognize the various effects that can alter the physical properties of the TMDCs in a sandwich geometry. Quite well known are the local strains and possible defect localization in TMDCs on pillars. While the uncontrolled occurrence of many defects is typically detrimental to material properties, carefully structured and induced defects and strain engineering have led to new applications, including single-photon sources in monolayer WSe_2 [18, 19, 20, 21, 45] and inducing direct bandgap in multilayer WSe_2 [22].

In addition, the charge transfer by the Ag sphere or Au disc into the material can result in doping of the material, resulting in a shift in the optical bandgap of the material, offering another important handle towards engineering the properties of TMDCs for applications [23, 24]. This has led to critical applications in spintronics, high-speed transistors, and various sensors [25–28]. Metal nanoparticles are known to reduce lifetime/speed up the decay process.

Surprisingly, there have been only a limited number of studies on the effects of doping and strain on WSe_2 characterized through PL and/or Raman shifts. These include a report on Niobium-induced p-doping of WSe_2 causing a redshift in PL energy as well as a Raman shift, while other p-dopants like Magic blue or $[N(C_6H_4\text{-}p\text{-}Br)_3]$ $SbCl_6$ causing a blueshift [28–31]. In other work, while p-doping by Au is established in the WSe_2 monolayer, the effect on PL energies has not been discussed [31].

With such an expanse of applications of TMDCs- plasmonic hybrid, here we present a careful investigation of the effect of a plasmonic cavity over WSe_2 as the TMDC, specifically for strain and doping consequences, using Raman and PL. The dimer-2D cavity was fabricated on pillar geometry to induce deterministic strain in WSe_2.

We modelled multiple plasmonic architectures to find one with resonance closest or equal to WSe_2. Few of such examples are shown in supplementary information figure S1. Keeping in mind the feasibility of fabrication over pillars and other factors, we chose a sphere-disc geometry to be fabricated over pillars. A plasmonic-2D material hybrid device geometry, as shown in figure 1(a), which is reasonably close to the final experimental device, is studied here in detail. We consider a silver (Ag) sphere of radius 75 nm and a gold (Au) disc of radius 100 nm, thickness 40 nm, separated by monolayer WSe_2 of thickness 0.7 nm, and simulated the scattering cross-section and electric field enhancement $|E/E_o|$ using Finite Element Method (FEM) based COMSOL simulations. The dielectric function values of WSe_2 were taken from Heinz *et al* [32]. The geometry parameters were chosen to have a resonance wavelength close to the WSe_2 optical bandgap at 750 nm. Figure 1(b) shows E/E_o field enhancement in the hotspot as high as 5000. Figure 1(c) shows the spatial extent of the electric field enhancement in the hot spot region, which lies within a few nanometers. The device fabrication and characterization details of the geometry are explained in the Experimental section below.

Results and discussion

To inspect the effect of the plasmonic hotspots over WSe_2 in our device geometry, we analyze the enhancement and shift in its Raman signal. Raman shift of bare monolayer WSe_2 has a peak ~250 cm^{-1} which corresponds to the degenerate $E^1_{2g} + A_{1g}$ in-plane vibration mode, and a peak ~260 cm^{-1} which corresponds to the 2LA(M) second-order mode [33, 34].

Figure 2(a) shows the Raman shift of monolayer WSe_2 with and without the plasmonic confinement. To rule out the effect of the heat-induced shift in the Raman spectra of WSe_2, we performed Raman measurements on W-bare sample before and after heating it at 260 C for 15 min figure S3 shows the respective Raman spectra with no difference in the mode position due to heating. To make a quantitative estimate of the enhancement of the electric field, we took the ratio of the total area under the $E^1_{2g} + A_{1g}$ Raman band as a measure of the strength of the Raman signal, following the method outlined by Paria *et al* [15]. Accordingly, the ratio of the area under the curve of $E^1_{2g} + A_{1g}$ peak of the sandwiched nanostructure to the area under the peak for bare WSe_2 on SiO_2/Si substrate provided an estimate of the plasmonic enhancement of ~2. For the theoretical estimation, we used the enhancement curve from the numerical simulation in figure 1(b). Theoretically, the net enhancement of the Raman signal for a laser focal spot of area A is given by

$$\left(\frac{|\mathrm{Ep}|}{|\mathrm{Epo}|}\right)^2_{\mathrm{abs}} \left(\frac{|\mathrm{Ep}|}{|\mathrm{Epo}|}\right)^2_{\mathrm{emi}} \left(\frac{\sigma}{\mathrm{A}}\right),$$

where $\left(\frac{|\,\mathrm{Ep}\,|}{|\,\mathrm{Epo}\,|}\right)^2_{\mathrm{abs}}$ is the enhancement due to the component of the strongly enhanced near field parallel (E_p) to WSe_2 at the wavelength of the excitation laser (532 nm), $\left(\frac{|\,\mathrm{Ep}\,|}{|\,\mathrm{Epo}\,|}\right)^2_{\mathrm{emi}}$ is the local electric enhancement at the Stokes-shifted emission wavelengths (539 nm). The area of high field enhancement (σ) is calculated by taking the fwhm of the in-plane enhanced fields. From figure 1(b), the primary source of the enhancement $\left(\frac{|\,\mathrm{Ep}\,|}{|\,\mathrm{Epo}\,|}\right)^2_{\mathrm{abs}}$ at the wavelength of the excitation laser (532 nm) was 81. The largely enhanced EM fields were concentrated in a tiny region of area $\sigma \approx 150\ nm^2$ at the junction of the 2D-plasmonic geometry, as shown in figure 1(c). The secondary source of enhancement $\left(\frac{|\,\mathrm{Ep}\,|}{|\,\mathrm{Epo}\,|}\right)^2_{\mathrm{emi}}$ was 121 (at 539 nm) for the E^1_{2g}+A_{1g} peak. Net estimated enhancement was, thus, ~1.4, which is reasonably close to the experimental value obtained above, proving that the plasmonic geometry indeed results in a hundred-fold focussing of optical intensity.

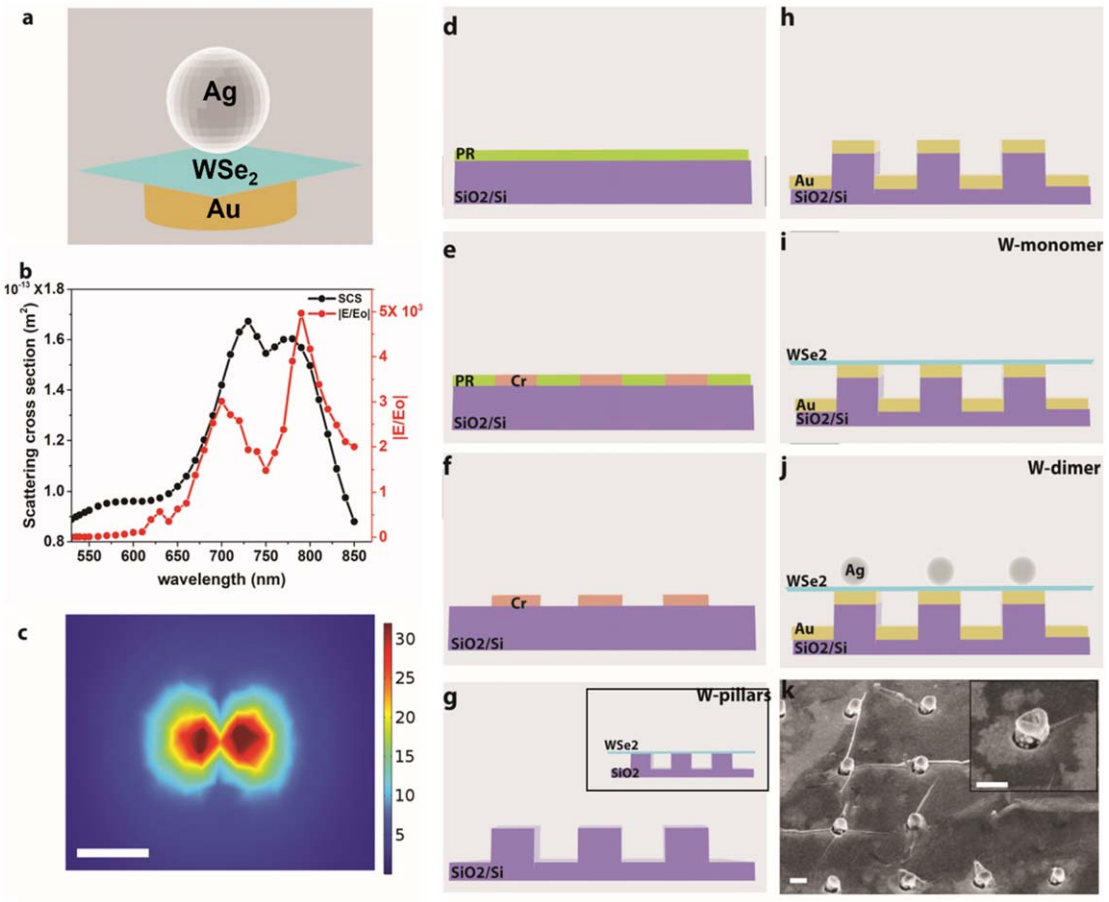

Figure 1. (a) Schematic of desired 2D-plasmonic hybrid geometry. (b) simulated scattering cross section and electric field enhancement for Ag/WSe_2/Au geometry. (c) Spatial confinement of local electric field enhancement hotspot at 750 nm. Scale bar 10 nm. (d–j) Schematic of fabrication technique used; (d) PMMA spin coated SiO_2/Si substrate for e-beam lithography, (e) patterned, developed and Cr deposited SiO_2/Si substrate, (f) PMMA lifted-off leaving Cr disc as mask for substrate etching, (g) SiO_2 etched and Cr removed pillars; Inset shows WSe_2 transferred on such a substrate for fabrication of W-pillars control sample, (h) Au film thermally evaporated on SiO_2/Si pillars, (i) WSe_2 transferred on Au-pillar substrate to form W-monomer control sample, (j) Ag/WSe_2/Au substrate post overlay lithography, development, Ag deposition, lift-off, and annealing steps. (k) SEM image of final fabricated device, inset shows a magnified image of single dimer-on-pillar structure with WSe_2. Scale bar 200 nm.

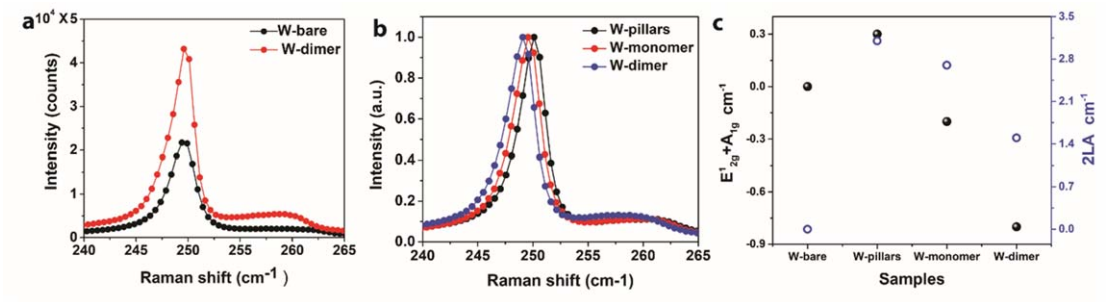

Figure 2. (a) Raman shift of bare WSe_2 on SiO_2/Si substrate and WSe_2 embedded in plasmonic Ag–Au cavity showing $E^1_{2g} + A_{1g}$ peak at 250 cm^{-1} and 2LA mode at 260 cm^{-1}. The area under the $E^1_{2g} + A_{1g}$ peak gives quantitative Raman plasmonic enhancement of the dimer system. (b) Normalised Raman spectra of the dimer and the control samples, W-pillars with WSe_2 on SiO_2/Si pillars and W-monomer with WSe_2 on Au disc on SiO_2 pillars. A clear redshift is observed in Raman peaks. (c) Summary of the shift in both $E^1_{2g} + A_{1g}$ and 2LA peaks for the control samples and device geometry.

We also studied the shift in the Raman bands and a comparison was drawn of the dimers with the control samples of WSe_2/SiO_2 pillar (W-pillar) geometry and WSe_2/Au Disc/SiO_2 pillar (W-monomer) geometry, both prepared using fabrication details mentioned in the experimental section. It was observed that addition of Au disc on WSe_2 redshifts the $E^1_{2g} + A_{1g}$ peak by 0.5 cm^{-1} compared to the W-pillar, while the 2LA peak shifts by

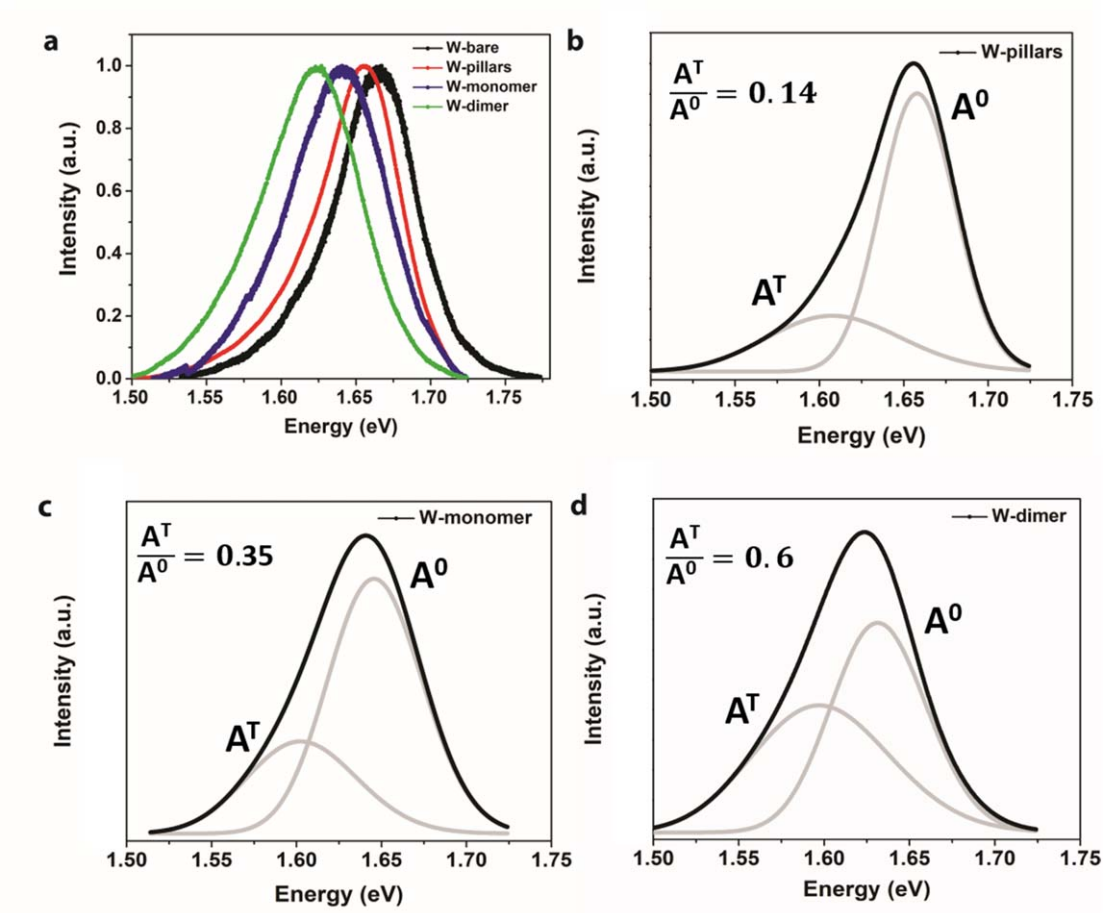

Figure 3. (a) PL spectra for bare WSe_2, pillar, monomer, and dimer samples. The latter three show redshift of 21–35 meV w.r.t the bare sample. Lorentzian fitting and deconvolution of PL peak to neutral exciton (A^0) ~1.66 eV and trion peak (A^*) ~1.63 eV for (b) WSe_2 on SiO_2 pillars (W-pillar) sample, (c)WSe_2 on Au disc on SiO_2 pillar (W-monomer) sample and (d) Ag/WSe_2/Au on SiO_2 pillar sample (W-dimer). Clearly, the trion peak increases in intensity relative to the neutral exciton peak as the doping increases.

1 cm^{-1}. This shift, shown in figure 2(b), is in accordance with previous work where monolayer WSe_2 decorated with Au nanoparticles showed a redshift in the $E^1_{2g} + A_{1g}$ peak [31]. Adding Ag on top of this monomer structure further redshifts the in-plane vibrational mode by 0.5 cm^{-1} compared to W-monomer and by 1 cm^{-1} compared to W-pillar. The 2LA mode also sees a significant redshift of 2 cm^{-1} (3 cm^{-1}) compared to its previous W-monomer (W-pillar) control geometry. This is one-of-a-kind reporting of the optical properties where the effect of silver on monolayer WSe_2 has been reported optically. The shifts have been summarised in figure 2(c). A similar reduction in the Raman shift of WSe_2 observed in previous works says that a tensile strain is induced on WSe_2 by our geometry [35–37]. The strain induced can be quantified using photoluminescence (PL) measurements. Raman does, however, establish that the strain induced is biaxial rather than uniaxial for the current device, as no splitting is observed in the $E^1_{2g} + A_{1g}$ peak [35].

We next carried out PL measurements on the dimer sample and control samples to understand the effect of charge transfer by Ag and Au onto WSe_2 in variable conditions and quantify the strain induced in WSe_2. Albeit doping through electrical control of carrier concentration is well established, such as through the application of voltage to the gate electrode, the purpose of this study was to understand the nature of doping induced by plasmonic materials in a transparent device architecture; followed by optical characterizations using PL [28–31]. Figure 3(a) shows photoluminescence (PL) spectra for W-bare, W-pillar, W-monomer, and W-dimer samples. The data has been normalized to accentuate the peak shifts. Pristine monolayer WSe_2 (W-bare) presents a prominent PL peak at 1.66 eV (A excitonic emission), corresponding to the direct bandgap transition. We find that the addition of Au to the device geometry redshifts the optical bandgap by 21 meV.

Interestingly, the addition of the top Ag sphere to the geometry further redshifts the optical bandgap by 14 meV (a total of 35 meV shift from pristine WSe_2). This material effect of Ag sphere onto monolayer WSe_2 has not been reported before to the best of our knowledge, and previous works have always associated redshift in PL of monolayer due to various dopants with p-doping of the material [28, 38–40]. Raman peak shift pattern observed matches with other work indicative of possible p-type doping of WSe_2 by our device structure;

however, a conclusive result would require an electrical measurement [31]. To investigate the effect of plasmonic parameters and structural variation on bandgap shift, we varied the diameter of the Au disc for W-monomer sample and the pillar diameter in W-pillar sample. Figure S2 in supplementary information shows that the PL peak position did not change dramatically in either case.

As established before, using Raman analysis, the type of strain acting on WSe_2 by our device is biaxial tensile; we quantified the amount of strain induced using the magnitude of peak shift values of PL spectra. We found that a strain of 0.2% and 0.3% was induced onto WSe_2 by the W-monomer and W-dimer geometry, respectively, following the work of Johari and Shenoy [41].

Apart from the PL peak position redshift, there was an apparent increase in the FWHM of the PL peak. An increase in FWHM is suggestive of other excitonic species formation. Hence, we deconvoluted the A exciton peak into the neutral exciton emission (A^0) at 1.66 eV and the trion (A^T) at ~1.63 eV for the TMDC using Lorentzian fitting [38, 42, 46]. This assignment of the trion peak to ~1.63 eV comes from works of Zhang R *et al* [38], Huang J *et al* [46] and Jones A.M. *et al* [43] who used optical and electrical measurements to assign the peaks. An accurate assignment would require altering the device to include electrical pads for gate measurements, which is out of the scope of this work. Figure S5 in supplementary information shows the FWHM of the A^0 and A^T peak for bare to dimer samples. Figures 3(b)–(d) shows deconvoluted trion and exciton peaks for the three samples; W-pillars, W-monomer, and W-dimer. The deconvoluted trion and exciton peak for the W-bare sample has been added as figure S6 in supplementary information. It can be seen that the neutral excitons (A^0) dominate the PL emission of W-pillars. But as we introduce Au and Ag in the system, the intensity ratio of trion to neutral exciton (A^T/A^0) increases, indicating the existence of enhanced concentrations of excess carriers through doping effects. However, the literature suggests similar modifications can also happen due to induced defects in the system [38, 46]. The ratio in our system changes from 0.14 for W-pillar to 0.35 for W-monomer and 0.6 for the W-dimer sample. This encouraging observation suggests an efficient material route toward bandgap engineering in WSe_2 for single-photon emitter-type device applications.

Conclusion

We investigated the effect of strain and metallic (Au, Ag) dopants on monolayer WSe_2 by sandwiching it in a raised plasmonic cavity. We found that both Raman and PL peak positions shift on the introduction of strain and Au, Ag. The Raman shift suggests the strain to be biaxial, and the PL suggests approximately 0.3%. The change in the ratio of trion to exciton peak intensity indicated doping effects of Au and Ag. The effect of structure and material on bandgap is relevant to photodetector applications, where 2D materials are coupled with plasmonic devices, e.g., when plasmonic nanoparticles [14–16] are in close proximity to the 2D photo-responsive material. In addition, these TMDC-plasmonic cavities, when strained, can be potential candidates toward deterministic and efficient sources of single photons for various quantum information applications.

Experimental section

Device fabrication

Fabrication of the base SiO_2 pillars on SiO_2/Si substrate was done using electron beam (e-beam) lithography. Photoresist (PR)PMMA 495k A4 was spin-coated on SiO_2/Si substrate. The desired hole pattern of radius 100 nm and pitch 1 μm was written and developed in MIBK: IPA solution for 1 min 35 s to obtain the hole array patterns in the PR. A 40 nm thick chromium (Cr) film was deposited on the hole pattern followed by lift-off to obtain 100 nm radius Cr discs. With Cr as a mask, the SiO_2 substrate was etched using Reactive Ion Etching (RIE) with CHF_3 gas forming SiO_2 pillars array. Cr was later removed using a Cr etchant, leaving arrays of 120–130 nm tall SiO_2 pillars, figure 1(f). A thin film of 40 nm Au thermally evaporated over the patterned pillar substrate formed the base plasmonic material of the dimer-on-pillar geometry, as shown in figure 1(g). Commercially available CVD grown monolayer WSe_2 (from Six-Carbon Technology) was transferred to the Au-SiO_2 pillar substrate using a standard PMMA-based wet transfer process. WSe_2-Au disc-SiO_2 pillar configuration or W-monomer obtained is shown in figure 1(h). Overlay e-beam lithography was used to expose only the top of the pillars covered with WSe_2/Au. Post-development, an array of holes was obtained precisely at the location of pillars. A 40 nm thick silver film was deposited, followed by lift-off leading to Ag disc-WSe_2-Au disc on SiO_2 pillar configuration. This was further annealed at 260 °C for 15 min in nitrogen ambient to form an Ag nanoparticle-WSe_2-Au disc configuration, denoted as W-dimer sample ahead. Figure 1(j) shows the SEM image of the final fabricated dimer-on-pillar geometry with WSe2 in between.

Optical characterizations

The optical characterizations of Raman and PL spectra of our samples were carried out using Horiba Jobin Vyon LabRAM HR spectrometer with excitation laser 532 nm, 100x objective of 0.9 NA. The effective spot size was 800 nm. The incident laser power was 50 μW, and spectra were collected with an integration time of 3 s for PL and 5 s for Raman. The signal was averaged three times for both. To confirm that input laser power used has no effect on the PL spectra, we performed power dependence of W-bare sample and found that spectra do not shift as a function of power for upto few 100 μW, as shown in figure S4.

Acknowledgments

We thank SERB for funding this research. We also acknowledge funding from MHRD, MeitY, and DST Nano Mission for supporting the facilities at CeNSE. We thank Dr Haobijam Johnson Singh for his inputs in the initial design of the experiment.

Data availability statement

The data that support the findings of this study are available upon reasonable request from the authors.

Conflicts of interest

There are no conflicts of interest to declare.

ORCID iDs

Priyanka Suri https://orcid.org/0000-0003-2204-6889
Preeti Deshpande https://orcid.org/0000-0002-2951-9856
Ambarish Ghosh https://orcid.org/0000-0002-2524-0014

References

[1] Oh Y J, Kang M, Park M and Jeong K H 2016 Engineering hot spots on plasmonic nanopillar arrays for SERS: A review *Biochip Journal* **10** 297–309
[2] Giannini V, Fernández-Domínguez A I, Heck S C and Maier S A 2011 Plasmonic nanoantennas: Fundamentals and their use in controlling the radiative properties of nanoemitters *Chem. Rev.* **111** 3888–912
[3] Gonçalves M R 2014 Plasmonic nanoparticles: fabrication, simulation and experiments *J. Phys. D: Appl. Phys.* **47**
[4] Jeong H H, Adams M C, Günther J P, Alarcón-Correa M, Kim I, Choi E, Miksch C, Mark A F, Mark A G and Fischer P 2019 Arrays of plasmonic nanoparticle dimers with defined nanogap spacers *ACS Nano* **13** 11453–9
[5] Sun C, Qin C, Zhai H, Zhang B and Wu X 2021 Optical properties of plasma dimer nanoparticles for solar energy absorption *Nanomaterials* **11**
[6] Vazquez-Mena O, Sannomiya T, Villanueva L G, Voros J and Brugger J 2011 Metallic nanodot arrays by stencil lithography for plasmonic biosensing applications *ACS Nano* **5** 844–53
[7] Kuznetsov A I, Evlyukhin A B, Goṇalves M R, Reinhardt C, Koroleva A, Arnedillo M L, Kiyan R, Marti O and Chichkov B N 2011 Laser fabrication of large-scale nanoparticle arrays for sensing applications *ACS Nano* **5** 4843–9
[8] Sun Y, Gao S and Xie Y 2014 Atomically-thick two-dimensional crystals: electronic structure regulation and energy device construction *Chem. Soc. Rev.* **43** 530–46
[9] Zhao J, Jin X, Vdovenko M, Zhang L, Sakharov I Y and Zhao S 2015 A WS_2 nanosheet based chemiluminescence resonance energy transfer platform for sensing biomolecules *Chem. Commun.* **51** 11092–5
[10] Tan C, Liu Z, Huang W and Zhang H 2015 Non-volatile resistive memory devices based on solution-processed ultrathin two-dimensional nanomaterials *Chem. Soc. Rev.* **44** 2615–28
[11] Bernardi M, Palummo M and Grossman J C 2013 Extraordinary Sunlight absorption and one nanometer thick photovoltaics using two-dimensional monolayer materials *Nano Lett.* **13** 3664–70
[12] Eda G and Maier S A 2013 Two-dimensional crystals: managing light for optoelectronics *ACS Nano* **7** 5660–5
[13] Tedstone A A, Lewis D J and O'Brien P 2016 Synthesis, properties, and applications of transition metal-doped layered transition metal dichalcogenides *Chem. Mater.* **28** 1965–74
[14] Ghosh P, Paria D, Balasubramanian K, Ghosh A, Narayanan R and Raghavan S 2019 Directed microwave-assisted self-assembly of Au–graphene–au plasmonic dimers for SERS applications *Adv. Mater. Interfaces* **6** 1–9
[15] Paria D, Roy K, Singh H J, Kumar S, Raghavan S, Ghosh A and Ghosh A 2015 Ultrahigh field enhancement and photoresponse in atomically separated arrays of plasmonic dimers *Adv. Mater.* **27** 1751–8
[16] Deshpande P, Suri P, Jeong H H, Fischer P, Ghosh A and Ghosh A 2020 Investigating photoresponsivity of graphene-silver hybrid nanomaterials in the ultraviolet *J. Chem. Phys.* **152**
[17] Echtermeyer T J, Britnell L, Jasnos P K, Lombardo A, Gorbachev R V, Grigorenko A N, Geim A K, Ferrari A C and Novoselov K S 2011 Strong plasmonic enhancement of photovoltage in graphene *Nat. Commun.* **2** 0–4
[18] Palacios-Berraquero C, Kara D M, Montblanch A R P, Barbone M, Latawiec P, Yoon D and Atatüre M 2017 Large-scale quantum-emitter arrays in atomically thin semiconductors *Nat. Commun.* **8** 1–6

[19] Tripathi L N, Iff O, Betzold S, Dusanowski Ł, Emmerling M, Moon K and Schneider C 2018 Spontaneous emission enhancement in strain-induced WSe2 Monolayer-based quantum light sources on metallic surfaces *ACS Photonics* **5** 1919–26
[20] Iff O, Tedeschi D, Martín-Sánchez J, Moczała-Dusanowska M, Tongay S, Yumigeta K and Schneider C 2019 Strain-tunable single photon sources in WSe2 monolayers *Nano Lett.* **19** 6931–6
[21] Koperski M, Nogajewski K, Arora A, Cherkez V, Mallet P, Veuillen J Y and Potemski M 2015 Single photon emitters in exfoliated WSe2 structures *Nat. Nanotechnol.* **10** 503–6
[22] Desai S B, Seol G, Kang J S, Fang H, Battaglia C, Kapadia R and Javey A 2014 Strain-induced indirect to direct bandgap transition in multilayer WSe 2 *Nano Lett.* **14** 4592–7
[23] Fang H, Chuang S, Chang T C, Takei K, Takahashi T and Javey A 2012 High-performance single layered WSe 2 p-FETs with chemically doped contacts *Nano Lett.* **12** 3788–92
[24] Iqbal M W, Elahi E, Amin A, Hussain G and Aftab S 2020 Chemical doping of transition metal dichalcogenides (TMDCs) based field effect transistors: A review *Superlattices Microstruct.* **137** 106350
[25] Xiao D, Liu G, Bin, Feng W, Xu X and Yao W 2012 Coupled spin and valley physics in monolayers of MoS_2 and other group-VI dichalcogenides *Phys. Rev. Lett.* **108** 1–5
[26] Yuan H, Bahramy M S, Morimoto K, Wu S, Nomura K, Yang B J and Iwasa Y 2013 Zeeman-type spin splitting controlled by an electric field *Nat. Phys.* **9** 563–9
[27] Lopez-Sanchez O, Lembke D, Kayci M, Radenovic A and Kis A 2013 Ultrasensitive photodetectors based on monolayer MoS 2 *Nat. Nanotechnol.* **8** 497–501
[28] Nam H J, Kim J and Park J H 2017 Wide-range controllable doping of tungsten diselenide (WSe_2) based on hydrochloric acid treatment *J. Phys. Chem. C* **121** 14367–72
[29] Pandey S K, Alsalman H, Azadani J G, Izquierdo N, Low T and Campbell S A 2018 Controlled p-type substitutional doping in large-area monolayer WSe2 crystals grown by chemical vapor deposition *Nanoscale* **10** 21374–85
[30] Zhang S, Hill H M, Moudgil K, Richter C A, Hight Walker A R, Barlow S and Pookpanratana S J 2018 Controllable, wide-ranging n-doping and p-doping of monolayer group 6 transition-metal disulfides and diselenides *Adv. Mater.* **30**
[31] Chen C H, Wu C L, Pu J, Chiu M H, Kumar P, Takenobu T and Li L J 2014 Hole mobility enhancement and p-doping in monolayer WSe2 by gold decoration *2D Mater.* **1**
[32] Li Y, Chernikov A, Zhang X, Rigosi A, Hill H M, van der Zande A M, Chenet D A, Shih E-M, Hone J and Heinz T F Measurement of the optical dielectric function of monolayer transition-metal dichalcogenides: MoS_2, $MoSe_2$, WS_2, and WSe_2 *Phys. Rev. B* **90** 205422
[33] Tonndorf P *et al* Photoluminescence emission and Raman response of monolayer MoS2, MoSe2, and WSe2 *Opt. Express* **21** 4908–16 2013
[34] Zhao W, Ghorannevis Z, Amara K K, Pang J R, Toh M, Zhang X and Eda G 2013 Lattice dynamics in mono- and few-layer sheets of WS2 and WSe2 *Nanoscale* **5** 9677–83
[35] Sahin H, Tongay S, Horzum S, Fan W, Zhou J, Li J and Peeters F M 2013 Anomalous Raman spectra and thickness-dependent electronic properties of WSe2 *Physical Review B - Condensed Matter and Materials Physics* **87** 1–6
[36] Chang C H, Fan X, Lin S H and Kuo J L 2013 Orbital analysis of electronic structure and phonon dispersion in MoS 2, MoSe2, WS2, and WSe2 monolayers under strain *Physical Review B - Condensed Matter and Materials Physics* **88** 1–9
[37] Amin B, Kaloni T P and Schwingenschlögl U 2014 Strain engineering of WS_2, WSe_2, and WTe2 *RSC Adv.* **4** 34561–5
[38] Zhang R, Drysdale D, Koutsos V and Cheung R 2017 Controlled layer thinning and p-type doping of WSe2 by Vapor XeF2 *Adv. Funct. Mater.* **27** 1702455
[39] Kim J E, Kang W T, Vu V T, Kim Y R, Shin Y S, Lee I, Won U Y, Lee B H, Kim K, Phan T L, Lee Y H and Yu W J 2021 Ideal PN photodiode using doping controlled WSe_2–$MoSe_2$ lateral heterostructure *J. Mater. Chem. C* **9** 3504–12
[40] Murai Y, Zhang S, Hotta T, Liu Z, Endo T *et al* 2021 Versatile post-doping toward two-dimensional semiconductors *ACS Nano* **15** 19225–32
[41] Johari P and Shenoy V B 2012 Tuning the electronic properties of semiconducting transition metal dichalcogenides by applying mechanical strains *ACS Nano* **6** 5449–56
[42] McCreary K M, Hanbicki A T, Sivaram S V and Jonker B T 2018 A- and B-exciton photoluminescence intensity ratio as a measure of sample quality for transition metal dichalcogenide monolayers *APL Mater.* **6** 111106
[43] Jones A M *et al Nat. Nano-Technol.* 2013 **8** 634
[44] Radisavljevic B, Radenovic A, Brivio J, Giacometti V and Kis A 2011 Single-layer MoS_2 transistors *Nat. Nanotechnol.* **6** 147–50
[45] Kern J, Niehues I, Tonndorf P, Schmidt R, Wigger D, Schneider R and Bratschitsch R 2016 Nanoscale positioning of single-photon emitters in atomically thin WSe_2 *Adv. Mater.* **28** 7101–5
[46] Huang J, Hoang T B and Mikkelsen M H 2016 Probing the origin of excitonic states in monolayer WSe2 *Scientific Reports* **6**